THIS IS AN EARLY ACCESS ARTICLE.
This article has been accepted for publication in a future issue of this journal,
but has not been fully edited. Content may change prior to final publication.

BULLETIN OF THE POLISH ACADEMY OF SCIENCES
TECHNICAL SCIENCES
DOI: 10.24425/bpasts.2027.7723

Vibration Damping of Thin-Walled Metal Sheets Using Paint Coatings

Wojciech Żyłka[1*], Marcin Pater[2], Monika Lubas[3], Stanisław Adamiak[1], Robert Wielgat[4]

[1] Institute of Materials Engineering, Faculty of Exact and Technical Sciences, University of Rzeszow, Pigonia 1, 35-310 Rzeszow, Poland
[2] Institute of Computer Science, Faculty of Exact and Technical Sciences, University of Rzeszow, Pigonia 1, 35-310 Rzeszow, Poland
[3] Department of Aerospace Engineering, Faculty of Mechanical Engineering and Aeronautics, Rzeszow University of Technology, 35-959 Rzeszow, Poland
[4] Department of Electronics and Smart Technologies, Faculty of Technical Sciences, University of Applied Sciences in Tarnow, Mickiewicza 8, 33-100 Tarnow, Poland

* Corresponding author: wzylka@ur.edu.pl

Abstract. In this study, the effect of three types of paint coatings, zinc, white camouflage SPR1001, and red rubber, on the vibration damping of thin-walled steel sheets was experimentally evaluated. Dynamic response measurements were performed using a Polytec PDV-100 laser vibrometer with chirp excitation in the frequency range from 1 to 500 Hz. The analysis was carried out in the frequency domain by determining changes in resonant frequencies and vibration amplitudes in the main vibration modes at approximately 65 Hz, 300 Hz, and in the high-frequency range. All tested coatings caused a clear reduction in vibration amplitude in the resonant frequency range. However, the investigated coatings did not act through the same dynamic mechanism. The zinc and red rubber coatings reduced the resonance amplitudes while causing only minor shifts in resonant frequencies, which is consistent with a damping-related mechanism inferred from the observed amplitude reduction. In contrast, the SPR1001 coating produced the strongest amplitude reduction but also a noticeable decrease in the natural frequencies due to its much larger mass increase, indicating a combined damping and mass-loading effect. These results show that thin paint coatings may serve not only as passive damping treatments, but also as a means of tailoring the dynamic response of thin-walled sheet components depending on whether the design priority is amplitude reduction alone or amplitude reduction combined with resonance retuning. To complement the dynamic analysis, additional microhardness measurements of selected paint coatings were performed, allowing a quantitative evaluation of their stiffness and deformation behaviour.

Key words: vibration damping; thin-walled structures; viscoelastic coatings; modal analysis; harmonic response; finite element method

1. INTRODUCTION

The issue of vibration damping in thin-walled metal components is of significant importance in the design and operation of engineering structures. Such elements, widely used in the automotive, aerospace, and household appliance industries, are characterized by a low level of internal damping, which means that even small dynamic excitations may lead to resonance phenomena with high amplitudes [1],[2],[3],[4],[5]. This results not only in excessive noise and reduced user comfort, but also in accelerated fatigue wear of the structure [6]. Energy-based approaches have been successfully applied to characterize fatigue failure under random loading conditions, demonstrating the close relationship between cyclic loading, energy dissipation, and fatigue damage accumulation [7]. Combined experimental–numerical approaches have also proved useful for predicting the fatigue lifetime of structural elements, providing a broader structural-performance context for the analysis of dynamically loaded components [8]. Similar dynamic requirements, including motion repeatability and vibration control, are also encountered in mechatronic and pneumatic systems [9, 10]. Numerous methods for reducing vibrations and noise in thin-walled structures have been proposed in the literature. The most commonly used approaches include active methods, such as active vibration control systems, semi-active methods, and passive methods [11],[12],[13],[14]. Among them, passive methods are of particular interest because of their simplicity, low cost, and operational reliability. One of the simplest and at the same time

effective solutions is the application of polymer or paint coatings to the surface of a component. Coatings of this type act as thin viscoelastic layers, introducing additional mechanisms of vibration energy dissipation [15]. Vibration energy is converted into heat through local shear deformation and internal friction within the coating [16, 17]. Even a thin layer of paint or polymer may cause a significant reduction in resonance amplitudes without noticeable changes in the natural frequencies of the system [13, 14]. This effect results from the fact that the mass and stiffness of a thin coating are small compared with those of the tested component, whereas its ability to dissipate energy is significant. The effectiveness of such coatings depends not only on the increase in mass, but mainly on the ability of the layer to absorb and dissipate strain energy, which is controlled by the local mechanical properties of the film, including elastic modulus, hardness, and viscoelastic compliance. Therefore, in energetic terms based on modal strain energy, the modal loss factor of a multilayer system may be treated as a weighted average of the losses in the individual layers, with the weights determined by the elastic strain energy stored in each of them [16,18]. Similar requirements for stable and repeatable dynamic operation are also reported for pneumatic systems [19]. For thin viscoelastic layers, the dynamic mechanical properties of the film are of key importance, especially the complex elastic modulus or, equivalently, the shear modulus together with the corresponding loss factor. These parameters describe the ability of the material to dissipate energy at a given frequency and temperature. Maximum damping usually occurs near the glass transition, which means that the composition, degree of crosslinking, and filler content of the paint determine the balance between hardness, stiffness, and energy dissipation [17, 20, 21]. Related requirements for limiting dynamic loads are also encountered in systems operating under special conditions [22]. In practice, during the bending of a thin-walled component, the coating is subjected to a considerable degree of shear deformation. An increase in shear strain within the film, for example through appropriate selection of thickness and the modulus ratio between the layer and the substrate, enhances energy dissipation. At the same time, increasing the modulus mismatch between the coating and the substrate may improve damping while also changing the effective stiffness of the system, as directly demonstrated by models and analyses of damping coatings [23, 24, 25]. For this reason, there is usually an optimum thickness range. A layer that is too thin does not accumulate sufficient strain energy, whereas a layer that is too thick may reduce shear deformation or introduce a significant stiffness to mass contribution, thereby altering the dynamic response of the system [26, 27]. A multilayer system, for example a softer primer combined with a harder topcoat, may operate in a manner similar to classical constrained layer damping solutions, in which a viscoelastic layer is confined between two stiffer layers. In such a case, the stiffer outer layer induces more intensive shear deformation in the viscoelastic layer, which increases the dissipation of vibration energy in the form of heat, provided that the material of this layer exhibits high internal losses within the temperature and frequency range corresponding to the operating conditions [24],[25],[26],[27],[28],[29]. The effectiveness of damping coatings has been evaluated in various experimental studies using both acoustic and modal methods. In particular, the application of laser vibrometry enables non-contact and precise recording of the dynamic response of small-sized elements with a low vibration level [1, 30, 31]. This makes it possible to determine both resonant frequencies and damping parameters. Thin paint coatings provide a simple, effective, and economical method of passive vibration reduction in thin-walled steel components [15, 26, 32].

The durability and degradation of polymer materials used in functional components can also be evaluated using complementary analytical techniques [33].

The aim of this study was to determine how the type of coating and the increase in coating thickness affect the vibration response of thin-walled steel sheets, with particular emphasis on distinguishing amplitude reduction caused mainly by increased material losses from that accompanied by significant mass-induced shifts of resonant frequencies. Three coating systems (zinc, white SPR1001, and red rubber) were investigated in the uncoated, single-layer, and double-layer states. The novelty of the study lies in the comparative identification of two different coating-response regimes: coatings exhibiting amplitude reductions with only minor frequency shifts, suggesting a possible damping contribution, and coatings combining amplitude reduction with a pronounced mass-loading effect.

2. MATERIALS AND METHODS

Six sheet specimens made of electrical silicon steel (Fe–Si alloy with a silicon content of approximately 1.5 to 2.5 wt.%) were prepared, with dimensions of 40 × 90 × 0.25 mm. Each specimen was permanently marked and weighed in the initial state, referred to as "Clear", before the application of protective coatings. In the next stage, the first coating layer ("Layer 1") was applied to specimens No. 1 to 3 using three different coating materials: zinc spray paint (specimen No. 1), white SPR1001 paint (specimen No. 2), and a red rubber coating in aerosol form (specimen No. 3). After drying, each specimen was weighed again in order to determine the mass increase resulting from the applied coating layer (Table 1). To maintain identical boundary conditions during the measurements and to eliminate the influence of repeated coating application on the same substrate, the second coating layer ("Layer 2") was applied to separate specimens No. 4 to 6. In this series, the same types of coatings were used as in the first layer, and the measurements were carried out as an independent experimental series.

TABLE 1. Mass of the specimens and mass increase after the application of one and two coating layers

This article has been accepted for publication in a future issue of this journal, but has not been fully edited. Content may change prior to final publication.

No.	Coating	Initial mass [g]	Mass after coating [g]	Increase [g]	Increase [%]
1 layer of paint					
1	Zinc spray paint	9.153	9.2149	0.0619	0,68
2	White SPR1001 paint	9.0937	9.7804	0.6867	7.55
3	Red rubber spray coating	9.0969	9.2271	0.1302	1.43
2 layers of paint					
4	Zinc spray paint	9.1084	9.3496	0.2412	2.64
5	White SPR1001 paint	9.085	10.629	1.5440	17
6	Red rubber spray coating	9.1335	9.3223	0.1888	2.07

The mass measurement results revealed a significant variation in the mass increase of the specimens after the application of the first coating layer, depending on the type of paint used. The largest mass increase was observed for the white SPR1001 coating, reaching approximately 7.5% relative to the initial state. In the case of zinc paint and the red rubber coating, the mass increase was clearly smaller and ranged between approximately 0,7 and 1.5%. After the application of the second coating layer, these differences became even more pronounced. The total mass increase for the specimens coated with SPR1001 reached approximately 17%, whereas for the zinc paint and the red rubber coating it did not exceed 2 to 3%. In the next stage, the thickness of the applied paint coatings was measured using a BLUE Technology MGR-10-S-FE coating thickness gauge. The obtained results are summarized in Table 2.

TABLE 2. Summary of the coating thickness measurements for the investigated sheet specimen

Sheet number	Sample designation	Paint coating thickness [µm]
Layer 1		
1	Zinc spray paint	10
2	White SPR 1001 paint	80
3	Red rubber spray coating	10
Layer 2		
4	Zinc spray paint	20
5	White SPR 1001 paint	100
6	Red rubber spray coating	20

2.1. Measurement Setup

The housing of the vibration exciter was manufactured using 3D printing technology, with 100% infill density in order to ensure sufficient structural stiffness and to minimize its influence on the tested object. Two electromagnets responsible for generating the dynamic excitation were mounted inside the printed housing. The electromagnets were connected in such a way that they operated alternately: the upper electromagnet generated force during the positive (upper) half-cycle of the sinusoidal excitation signal, whereas the lower electromagnet operated during the negative (lower) half-cycle. This configuration made it possible to obtain symmetrical oscillatory excitation while maintaining control over the direction of the applied force. The system was powered by an amplifier operating within a range in which the response of the tested object remained linear. The schematic diagram of the developed vibration excitation system is presented in Fig. 1.

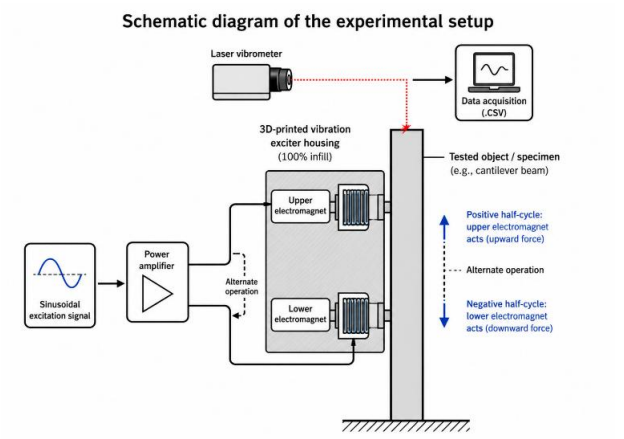


Fig.1. Schematic diagram of the experimental setup used for vibration excitation

The dynamic response of the specimens was measured using a Polytec PDV-100 laser Doppler vibrometer. The device enables non-contact measurement of surface vibration velocity along the axis of the laser beam. The recorded signal was subsequently analyzed in both the time and frequency domains using FFT analysis. Each specimen state was measured three times under unchanged mounting and excitation conditions. To assess experimental repeatability, the scatter of the principal resonance amplitudes was quantified using the sample standard deviation (SD) calculated from the three repeated measurements (n = 3), and the results are reported as mean ± SD.

2.2. Microhardness Measurements – Reference Coatings

To better interpret the influence of thin coating layers on the dynamic response of steel sheets, microhardness measurements using the nanoindentation method were performed. The microhardness measurements were performed for the same coating systems as those used in the vibration experiments, namely silver zinc spray paint, white SPR1001 paint, and red rubber spray coating. The measurements were performed using a CSM microhardness tester with the Vickers indentation method at a maximum load of 100 mN. Based on the analysis of the unloading curve–indentation depth using the Oliver–Pharr method, the following parameters were determined: indentation hardness (HIT), indentation modulus

This article has been accepted for publication in a future issue of this journal, but has not been fully edited. Content may change prior to final publication.

(EIT), maximum indentation depth (hmax), and creep deformation (CIT). For each configuration, a series of indentations was performed and average values were calculated. In this paper, the results are presented in the form of graphs (Section 4.4) without including the complete load–displacement curves. All measurements were conducted in accordance with ISO 14577-1 [34].

3. RESULTS AND DISCUSSION

3.1. Zinc spray paint

For the experiments, an aerosol zinc preparation in the form of a light-silver protective paint was used. The formulation contains finely dispersed particles of metallic zinc which, after application, form a compact and electrically conductive layer on the substrate surface. This layer provides cathodic protection, protecting the steel against corrosion processes (Fig. 2).

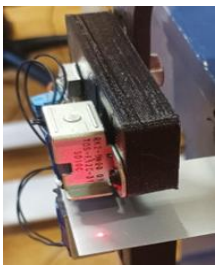


Fig.2. Measurement setup for the zinc spray paint coating

3.1.1. First measurement series – sheet specimen No. 1, comparison of Clear and Layer 1 states

The experiments were carried out on thin-walled metal specimens by analysing the dynamic response of the system before and after the application of a single layer of zinc spray paint. For each series, both the excitation and response waveforms were recorded by the PD2-MFS data acquisition card at a sampling frequency of 10 kHz for 30 s. The analogue output signal from the Polytec PDV-100 laser vibrometer was connected directly to the analogue input of the PD2-MFS card, without any external signal-conditioning or voltage-level-matching circuitry. The only amplification was provided by the internal electronics of the vibrometer head. According to the vibrometer documentation, the analogue output voltage range was ±4 V, whereas the data acquisition card operated with a 16-bit A/C converter and a fixed input voltage range of ±10 V. Although the vibrometer output occupied only approximately 40% of the fixed ±10 V input range of the PD2-MFS A/D converter, the resulting effective resolution of approximately 15 bits was sufficient for the present measurements and did not have a significant influence on the accuracy of the recorded vibration signals. The vibration response signal was then filtered using a 4th-order low-pass Butterworth digital filter with a cut-off frequency of 1 kHz. Afterwards, the FFT spectrum was computed using the MATLAB fft function, and the analysis of the obtained spectrum was limited to the frequency range of 0–500 Hz. For sheet specimen No. 1, three measurements were performed in the uncoated state (Clear) (Fig. 3) and three repetitions after the application of the first layer of zinc spray paint (Fig. 4).

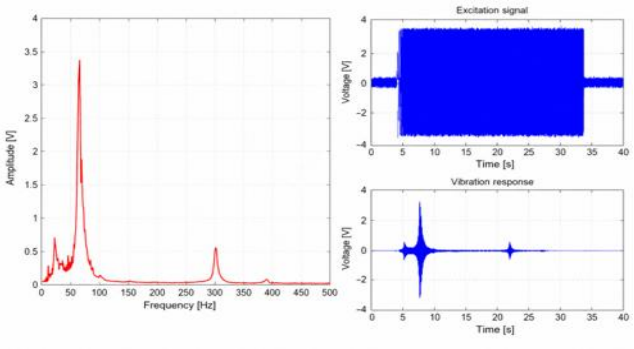


Fig.3. Example FFT amplitude spectrum for the Clear states along with the excitation signal and vibration response waveforms. Each state was measured in three repetitions.

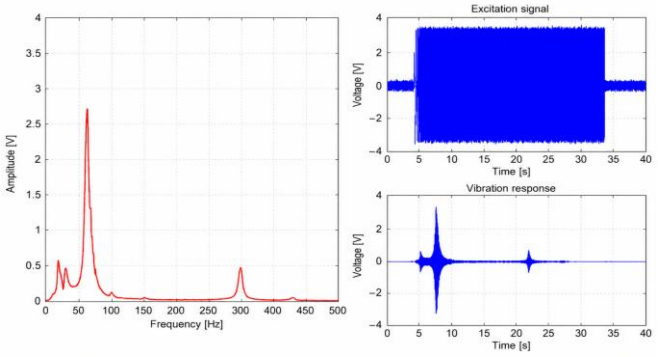


Fig.4. Example FFT amplitude spectrum for sheet specimen No. 1 after the application of the first layer of zinc spray paint (Layer 1) along with the excitation signal and vibration response waveforms. Each state was measured in three repetitions.

The spectral analysis (Figs. 3–4 and Table 3) revealed two principal resonances: 64–65 Hz (dominant mode) and 301–302 Hz. Throughout Tables 3–8, the notation f_i refers to the i-th resonance frequency (i=1,…,4), and A_i denotes the amplitude of the signal for the i-th resonance frequency. After the application of the first layer of zinc spray paint, no significant shift in the resonant frequencies was observed; however, the amplitudes decreased in all three repetitions. For the 64–65 Hz frequency range, the amplitude decreased from 3.27 ± 0.10 V to 2.76 ± 0.03 V (−15.5% averaged over three repetitions), while for the 301–302 Hz frequency range it decreased from 0.608 ± 0.055 V to 0.469 ± 0.006 V (−23.0%). An additional low-frequency component around 22 Hz also decreased from 0.699 V to 0.573 V (−18.0%) without any change in frequency. The nearly unchanged resonant frequencies, accompanied by reduced resonance amplitudes, suggest an increase in material losses introduced by the thin coating layer, while the global stiffness of the element remained essentially unchanged. This observation is consistent with the classical description of damping provided by thin viscoelastic layers [1, 14, 16, 17].

TABLE 3. Resonant frequencies and amplitudes for sheet specimen No. 1 (zinc spray paint) in the Clear and Layer 1 states

This article has been accepted for publication in a future issue of this journal, but has not been fully edited. Content may change prior to final publication.

Specimen state	f_1 [Hz]	A_1 [V]	f_2 [Hz]	A_2 [V]	f_3 [Hz]	A_3 [V]	f_4 [Hz]	A_4 [V]
Clear								
Measurement 1	22	0.709276	64	3.231558	302	0.598803	389	0.067388
Measurement 2	22	0.675445	64	3.198341	301	0.667202	390	0.064244
Measurement 3	22	0.712082	65	3.380794	302	0.559101	390	0.067180
Layer 1								
Measurement 1	22	0.571501	64	2.792849	302	0.461694	393	0.046128
Measurement 2	22	0.572208	65	2.734296	302	0.470035	393	0.048639
Measurement 3	22	0.574692	65	2.761149	302	0.473990	394	0.045490

Notation used in the table: f_i— frequency of the i-th resonance or characteristic spectral component ($i = 1, \ldots, 4$); A_i— corresponding signal amplitude.

3.1.2. Second measurement series (zinc spray paint, sheet specimen No. 4)

Similarly to sheet specimen No. 1, three measurements were performed for sheet specimen No. 4 in the following states: uncoated (Clear), after the first layer of zinc spray paint (L1), and after the second layer (L2). The frequency spectra revealed two stable resonances: a dominant mode in the range of 64–66 Hz and a higher mode in the range of 302–307 Hz (Table 4), as well as a weaker component near 395–400 Hz.

TABLE 4. Resonant frequencies and amplitudes for sheet specimen No. 4 (zinc spray paint) in the Clear, Layer 1, and Layer 2 states.

Specimen state	f_1 [Hz]	A_1 [V]	f_2 [Hz]	A_2 [V]	f_3 [Hz]	A_3 [V]	f_4 [Hz]	A_4 [V]
Clear								
Measurement 1	25	0.441750	65	2.849663	307	0.544068	398	0.081161
Measurement 2	25	0.445633	65	2.830272	306	0.509581	398	0.077424
Measurement 3	25	0.448111	65	2.828962	307	0.508068	398	0.081167
Layer 1								
Measurement 1	25	0.404639	65	2.676199	286	0.496211	400	0.055777
Measurement 2	25	0.406927	66	2.710719	286	0.493963	398	0.060201
Measurement 3	25	0.410167	65	2.737759	286	0.492824	398	0.055496
Layer 2								
Measurement 1	22	0.608135	64	2.662175	302	0.288698	396	0.046419
Measurement 2	22	0.600352	65	2.600549	302	0.289753	395	0.043961
Measurement 3	22	0.605431	65	2.600853	302	0.289368	396	0.044875

After the application of a single layer of zinc spray paint, the resonant frequencies remained practically unchanged, remaining close to 65.0 Hz, while for the higher mode a slight shift from 306.7 Hz to 304.7 Hz was observed. In contrast, the amplitudes decreased consistently: for the 64–65 Hz range from 2.84 ± 0.01 V to 2.71 ± 0.03 V (−4.5% on average across three repetitions) and for the band around 305 Hz from 0.521 V to 0.415 V (−20.4%). The application of two layers resulted in a further reduction of amplitudes with only minor frequency changes: for 64–65 Hz the amplitude decreased to 2.62 ± 0.04 V (a total reduction of −7.6% relative to the uncoated state; 65.0–64.67 Hz) and for approximately 302 Hz to 0.289 V (a total reduction of −44.4%). The component in the 395–400 Hz range also decreased (0.080 → 0.057 V after L1 and 0.045 V after L2). In the band around 25 Hz, a slight decrease was observed for L1 (0.445 → 0.407 V), whereas for L2 an increase to approximately 0.605 V was recorded. Due to the low frequency and its sensitivity to boundary conditions, this component was treated as auxiliary and was not included in the modal conclusions.

3.2. White camouflage paint SPR1001

The experiments were conducted on a steel specimen coated with a protective camouflage coating of the SPR1001 type, commonly used in the defence industry (Fig. 5). The coating contains anticorrosive pigments dispersed in a durable binder, enabling the formation of a uniform and well-adhering layer on the steel substrate. After curing, the coating exhibited high resistance to atmospheric factors and mechanical loads, while simultaneously acting as both an anticorrosive barrier and a camouflage coating.

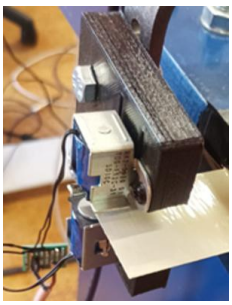


Fig.5. Measurement setup for the white SPR1001 coating.

3.2.1. First measurement series (white SPR1001 paint, sheet specimen No. 2)

The dynamic response of specimen No. 2 was compared in the uncoated state and after application of the first SPR1001 coating layer, with the results summarized in Table 5. The specimen responded to excitation in the frequency range of 0–500 Hz, with distinct components observed around 23 Hz, in the fundamental mode at 65–66 Hz, and in a higher mode at 303–304 Hz. Additionally, a high-frequency component at 397–398 Hz was visible. For the uncoated specimen, the highest amplitudes occurred in the fundamental mode (≈3.0 V) and in the higher mode (≈0.57–0.66 V). For the fundamental mode, the mean amplitude decreased from 3.00 ± 0.08 V in the Clear state to 2.71 ± 0.11 V after application of the first SPR1001 layer. For the higher resonance mode, the mean amplitude decreased from 0.638 ± 0.036 V in the Clear state to 0.383 ± 0.002 V after application of the first SPR1001 layer. After the application of the first SPR1001 layer, the resonant frequencies shifted toward lower values: 65–66 → 63 Hz (fundamental mode), 303–304 → 288 Hz (higher mode), 23 → 22 Hz, and 397–398 → 378–379 Hz. At the same time, the amplitudes in all these bands decreased in all three repetitions: to 2.63–2.84 V (63 Hz), 0.381–0.386 V (288 Hz), 0.519–0.528 V (22 Hz), and 0.051–0.065 V (378–379 Hz). The application of the coating therefore reduced the natural frequencies and lowered the level of resonant response.

This article has been accepted for publication in a future issue of this journal, but has not been fully edited. Content may change prior to final publication.

TABLE 5. Resonant frequencies and amplitudes for the specimen coated with white SPR1001 paint (sheet specimen No. 2)

Specimen state	f_1 [Hz]	A_1 [V]	f_2 [Hz]	A_2 [V]	f_3 [Hz]	A_3 [V]	f_4 [Hz]	A_4 [V]
Clear								
Measurement 1	23	0.610340	65	2.999616	304	0.660008	397	0.084056
Measurement 2	23	0.612564	66	3.083077	304	0.569146	398	0.093633
Measurement 3	23	0.611529	66	2.924825	303	0.650765	398	0.092473
Layer 1								
Measurement 1	22	0.527585	63	2.628419	288	0.385887	379	0.065245
Measurement 2	22	0.518655	63	2.835464	288	0.383180	378	0.051192
Measurement 3	22	0.528099	63	2.675260	288	0.380894	379	0.053149

3.2.2. Second measurement series (white SPR1001 paint, sheet specimen No. 5)

Specimen No. 5 was tested in the Clear, L1, and L2 states, and the results are summarized in Table 6.

TABLE 6. Resonant frequencies and amplitudes for specimen No. 5 in the uncoated state and after the application of one (L1) and two (L2) layers of white SPR1001 paint

Specimen state	f_1 [Hz]	A_1 [V]	f_2 [Hz]	A_2 [V]	f_3 [Hz]	A_3 [V]	f_4 [Hz]	A_4 [V]
Clear								
Measurement 1	22	0.602799	63	2.870187	302	0.599893	384	0.068871
Measurement 2	22	0.583023	63	2.887900	302	0.603285	384	0.077028
Measurement 3	22	0.613594	63	2.906808	302	0.606112	384	0.077430
Layer 1								
Measurement 1	21	0.572786	61	2.622589	286	0.496211	367	0.045561
Measurement 2	21	0.561507	61	2.679245	286	0.493963	367	0.045533
Measurement 3	21	0.565378	61	2.597480	286	0.492824	367	0.046463
Layer 2								
Measurement 1	20	0.465762	57	2.206262	270	0.287095	348	0.029818
Measurement 2	20	0.466605	57	2.187350	270	0.285745	348	0.029725
Measurement 3	20	0.467196	57	2.197277	270	0.288007	347	0.029501

Table 6 summarizes the resonant frequencies and amplitudes of the specimen coated with SPR1001 paint in three states: uncoated (Clear), after one layer (L1), and after two layers (L2). The results clearly confirm that the SPR1001 coating significantly affects both the vibration amplitudes and the resonant frequencies of the tested sheets. In all identified frequency bands, the frequencies decrease, while the amplitudes are systematically reduced in the sequence Clear → Layer 1 → Layer 2. In the fundamental mode (63 → 61 → 57 Hz) and in the higher mode (302 → 286 → 270 Hz), the decrease in frequency corresponds to the increasing mass of the coating (a total increase of +17%). At the same time, the amplitudes in these bands decrease by approximately 10–25% after the first layer and by 20–50% after the second layer. For the fundamental mode, the mean amplitude decreased from 2.89 ± 0.02 V in the Clear state to 2.63 ± 0.04 V after the first layer and to 2.20 ± 0.01 V after the second layer. For the higher resonance mode, the mean amplitude decreased from 0.603 ± 0.003 V in the Clear state to 0.494 ± 0.002 V after the first layer and to 0.287 ± 0.001 V after the second layer. A particularly important trend is observed in the high-frequency band: the resonant frequency decreases from 384 Hz (Clear) to 367 Hz (L1) and to 347–348 Hz (L2), accompanied by a reduction in amplitude from 0.07 V to 0.03 V. This behaviour is consistent with the classical mass effect and confirms the predictable nature of the changes introduced by the coating. The results indicate that the SPR1001 paint exhibits the strongest influence on vibration reduction of the specimen, both through an increase in material losses and through the largest mass effect among the investigated coatings.

3.3. Red rubber spray coating

The influence of a red rubber spray coating on the dynamic response of thin-walled steel sheets was analysed. The coating was applied in the form of a liquid rubber layer using spray deposition. After application and solvent evaporation, the coating formed a continuous and flexible elastomeric layer (Fig. 6).

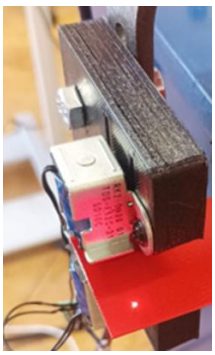


Fig.6. Measurement setup for the red rubber spray coating

3.3.1. First measurement series (red rubber spray coating, sheet specimen No. 3)

Two states were analysed: Clear (3×) and L1 (3×). Spectral analysis for the specimen coated with the red paint (Clear vs L1) reveals four repeatable frequency bands: approximately 33 Hz, 65 Hz, 302–305 Hz, and 393–396 Hz (Table 7). After the application of the first layer, the locations of the resonances remain practically unchanged or shift slightly toward lower frequencies: 65 → 64 Hz (−1 Hz), 305 → 302 Hz (−3 Hz), and 396 → 393–394 Hz (−2–3 Hz), while the band around 33 Hz remains at 33 Hz. In all three repetitions, the amplitudes in the L1 state are lower than in the uncoated state. For the 65 Hz band, the values decrease from 3.226–3.527 V to 2.634–2.888 V (reductions of approximately 17–18%). For the fundamental mode, the mean amplitude decreased from 3.37 ± 0.15 V in the Clear state to 2.76 ± 0.13 V after application of the first red rubber coating layer. In the region of 302–305 Hz, a decrease from 0.631–0.666 V to 0.513–0.625 V is observed (from a small reduction up to about

This article has been accepted for publication in a future issue of this journal, but has not been fully edited. Content may change prior to final publication.

23%, depending on the repetition). For the higher resonance mode, the mean amplitude decreased from 0.645 ± 0.019 V in the Clear state to 0.551 ± 0.064 V after application of the first red rubber coating layer. For the high-frequency component at 393–396 Hz, the amplitude decreases from 0.095–0.107 V to 0.0467–0.0614 V (a reduction of about 36–56%). In the band around 33 Hz, the level decreases from 1.104–1.189 V to 0.884–1.022 V (approximately 9–21%). These results indicate that a single layer of red coating significantly reduces the response over the entire analysed frequency range, with only small and expected shifts in the resonant frequencies.

Table 7. Resonant amplitudes for specimen No. 3 (three repetitions): uncoated state and after the first layer of red paint

Specimen state	f_1 [Hz]	A_1 [V]	f_2 [Hz]	A_2 [V]	f_3 [Hz]	A_3 [V]	f_4 [Hz]	A_4 [V]
Clear								
Measurement 1	33	1.119162	65	3.226923	305	0.666310	396	0.095077
Measurement 2	33	1.103856	65	3.527028	305	0.630806	396	0.107002
Measurement 3	33	1.188670	65	3.345434	305	0.639203	396	0.101333
Layer 1								
Measurement 1	33	0.883707	64	2.633755	302	0.515282	394	0.046717
Measurement 2	33	0.891738	64	2.887617	302	0.512932	393	0.055225
Measurement 3	33	1.021513	64	2.768699	302	0.625301	393	0.061433

3.3.2. Second measurement series (red spray coating, sheet specimen No. 6)

Specimen No. 6 was tested in the Clear, L1, and L2 states under unchanged mounting and excitation conditions. The resonant frequencies and amplitudes for the Clear, L1, and L2 states are summarized in Table 8.

TABLE 8. Resonant frequencies and amplitudes for sheet specimen No. 6 in the uncoated state and after the application of one and two layers of red paint.

Specimen state	f_1 [Hz]	A_1 [V]	f_2 [Hz]	A_2 [V]	f_3 [Hz]	A_3 [V]	f_4 [Hz]	A_4 [V]
Clear								
Measurement 1	22	0.613705	64	3.129124	302	0.578317	387	0.090464
Measurement 2	22	0.689188	63	3.106052	302	0.551317	387	0.084681
Measurement 3	22	0.6052	64	3.016105	302	0.57788	387	0.085672
Layer 1								
Measurement 1	23	0.519703	65	2.532318	301	0.481044	395	0.059217
Measurement 2	22	0.52128	65	2.571917	302	0.484734	395	0.059691
Measurement 3	22	0.521705	65	2.519199	302	0.484392	395	0.059837
Layer 2								
Measurement 1	22	0.511979	65	2.426945	300	0.4137	394	0.045435
Measurement 2	22	0.513823	65	2.422004	300	0.412878	394	0.046222
Measurement 3	22	0.513744	65	2.421715	300	0.414027	394	0.044857

Spectral analysis (Table 8) confirms the presence of four frequency bands: a low-frequency component (~22 Hz), the fundamental mode (approximately 63–65 Hz), a higher mode (approximately 300–302 Hz), and a high-frequency component (around 390 Hz). In the uncoated state, the spectra exhibit stable resonant frequencies. After the application of the first layer (L1), the frequencies remain similar or shift slightly by a few hertz. After the second layer (L2), this trend persists. The frequency changes are small and consistent with the mass effect. The amplitudes decrease consistently in the order Clear > L1 > L2 across all four bands. In the fundamental mode, the decrease is clearly visible already after L1 and becomes more pronounced after L2. For the fundamental mode, the mean amplitude decreased from 3.08 ± 0.06 V in the Clear state to 2.54 ± 0.03 V after the first layer and to 2.44 ± 0.02 V after the second layer. In the band around 300 Hz, the reduction is also significant and monotonic (Clear → L1 → L2). For the higher resonance mode, the mean amplitude decreased from 0.569 ± 0.015 V in the Clear state to 0.483 ± 0.002 V after the first layer and to 0.414 ± 0.001 V after the second layer. The high-frequency component near ~390 Hz shows the largest relative reduction after L2, whereas the ~22 Hz component decreases to a smaller but still consistent extent. These results indicate that the red rubber-type coating reduces vibration amplitudes with only minor changes in resonant frequencies, suggesting a possible contribution from increased energy dissipation.

4. COMPARISON OF THE INFLUENCE OF PAINT COATINGS ON VIBRATION REDUCTION (FFT ANALYSIS) AND MICROHARDNESS

The comparative analysis shows that the investigated coatings represent two different vibration-reduction regimes. The zinc and red rubber coatings exhibit amplitude-reduction behaviour consistent with increased damping, as they reduce the resonance amplitudes while causing only minor shifts in resonant frequencies. In contrast, the SPR1001 coating combines amplitude reduction with a clear downward shift of the resonance spectrum, which indicates a stronger mass-loading effect in addition to damping. This distinction is important from a design point of view, because it shows that similar amplitude reduction may be achieved through different dynamic mechanisms.

4.1. Zinc spray paint

The averaged FFT spectra confirm that the zinc coating reduces resonance amplitudes while causing only minor shifts in resonant frequencies, consistent with its relatively small mass increase (Fig. 7).

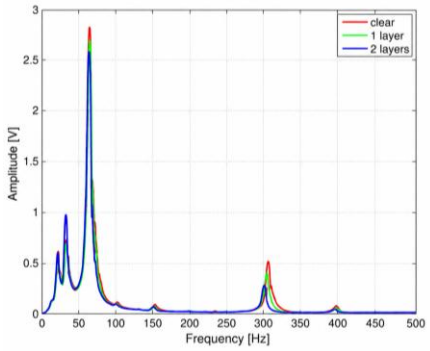


Fig.7. Comparison of FFT amplitude spectra for the specimen coated with zinc paint in the following states: uncoated (clear), one layer, and two layers.

This article has been accepted for publication in a future issue of this journal, but has not been fully edited. Content may change prior to final publication.

Averaged values from three measurement repetitions (n = 3) are shown for each state

4.2. White SPR1001 paint

Compared with the other coatings, the SPR1001 system is characterized by the largest increase in mass and thickness, which is reflected in more pronounced changes in the dynamic response. With successive layers, a reduction in resonant amplitudes is observed together with a tendency for the resonant frequencies to decrease, particularly for the fundamental mode in the region of approximately 65 Hz. This suggests a significant contribution of the mass-loading effect, potentially accompanied by increased energy dissipation in the coating. A comparison of the averaged FFT amplitude spectra (n = 3) for the specimen coated with white SPR1001 paint in the following states: uncoated (clear), one layer, and two layers is presented in Fig. 8.

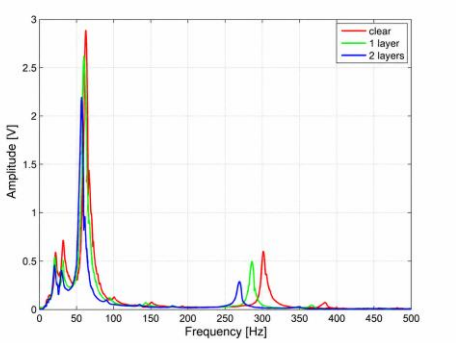


Fig.8. Comparison of FFT amplitude spectra for the specimen coated with white SPR1001 paint in the following states: uncoated (clear), one layer, and two layers. Averaged values from three measurement repetitions (n = 3) are shown for each state.

4.3. Red rubber-type coating (spray)

The averaged FFT spectra confirm that the red rubber coating reduces resonance amplitudes while causing only minor changes in resonant frequencies, suggesting a damping-related contribution to the observed amplitude reduction (Fig. 9).

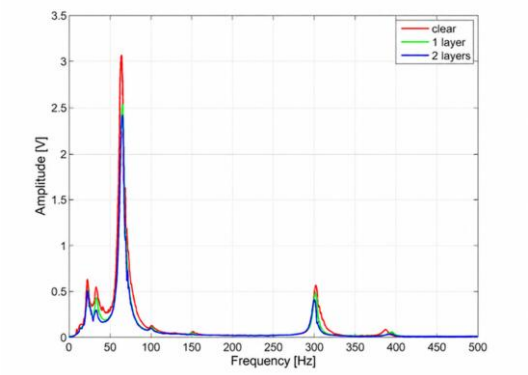


Fig.9. Comparison of FFT amplitude spectra for the specimen coated with the red rubber-type paint (spray) in the following states: uncoated (clear), one layer, and two layers.

4.4. Mechanical characterization of paint coatings (microhardness)

Microhardness measurements were performed for the same paint coatings as those used in the vibration damping tests, i.e., the silver zinc spray paint, the white SPR1001 paint, and the red rubber spray coating. The measurements were carried out for specimens coated with one and two layers; however, the results presented in Table 9 and discussed below refer to the single-layer coatings. The measurements were carried out by instrumented indentation using a Vickers indenter at a maximum load of 100 mN. The indentation hardness (HIT), indentation modulus (EIT), and indentation creep (CIT) were determined using the Oliver–Pharr method. The results are summarized in Table 9. The indentation hardness HIT is presented in Fig. 10, the indentation modulus EIT in Fig. 11, and the indentation creep CIT in Fig. 12.

TABLE 9. Microhardness parameters of the paint coatings used in the vibration tests.

Coating system	Specimen state	HIT [MPa]	EIT [GPa]	CIT [%]
Silver zinc spray paint	Specimen without number	197.04 ± 27.19	18.49 ± 1.94	23.69 ± 3.68
White SPR1001 paint	Specimen without number	4.51 ± 1.20	1.77 ± 0.30	55.13 ± 12.25
Red rubber-type spray coating	Specimen without number	45.45 ± 4.49	6.68 ± 0.50	37.89 ± 4.50

At the maximum indentation load of 100 mN, the mean maximum penetration depth hmax was 4.67 ± 0.32 µm for the zinc coating, 30.93 ± 3.63 µm for the SPR1001 coating, and 9.26 ± 0.48 µm for the red rubber coating. Relative to the corresponding single-layer coating thicknesses of approximately 10, 40, and 10 µm, respectively, these values correspond to hmax/thickness ratios of approximately 0.47, 0.77, and 0.93. The relatively large penetration-to-thickness ratios, particularly for the softer polymer coatings, indicate that the measured indentation parameters may be affected by the underlying steel substrate. Therefore, the HIT, EIT, and CIT values should be interpreted primarily as comparative parameters of the investigated coating systems rather than as intrinsic bulk-material properties. It should be emphasized that the indentation hardness, indentation modulus, and indentation creep provide complementary local mechanical information on the investigated coatings and should not be interpreted as direct measures of their dynamic viscoelastic damping behaviour. The obtained results indicate clear differences in the local mechanical properties of the investigated coatings. The silver zinc coating exhibited the highest indentation hardness and the highest indentation modulus among all analysed systems. The mean hardness was HIT = 197.04 ± 27.19 MPa, while the indentation modulus was EIT = 18.49 ± 1.94 GPa. At the same time, the indentation creep was the lowest among the tested coatings and amounted to CIT = 23.69 ± 3.68%. The zinc-rich coating formed a relatively hard and stiff surface layer, with a limited contribution of time-dependent deformation. This result is consistent with the vibration tests, in which the zinc coating

This article has been accepted for publication in a future issue of this journal, but has not been fully edited. Content may change prior to final publication.

reduced the resonance amplitudes while causing only slight shifts in the resonance frequencies. The white SPR1001 coating exhibited the lowest hardness and the lowest indentation modulus among the investigated coating systems. The mean indentation hardness was HIT = 4.51 ± 1.20 MPa, and the indentation modulus was EIT = 1.77 ± 0.30 GPa. The indentation creep was high and amounted to CIT = 55.13 ± 12.25%. These results indicate that the SPR1001 coating is a soft and compliant coating system, with a large contribution of time-dependent deformation. This behaviour is consistent with the dynamic measurements, in which the SPR1001 coating caused not only a reduction in vibration amplitudes but also a noticeable downward shift in the resonance frequencies. Therefore, in the case of SPR1001, the damping effect was accompanied by a distinct mass-loading effect and an effect related to the compliance of the coating. The red rubber spray coating exhibited intermediate mechanical properties. The hardness was HIT = 45.45 ± 4.49 MPa, and the indentation modulus was EIT = 6.68 ± 0.50 GPa, with an indentation creep of CIT = 37.89 ± 4.50%. These results confirm the elastomeric and viscoelastic character of the red coating. Compared with the zinc coating, the red rubber coating was softer and more susceptible to time-dependent deformation. Compared with the SPR1001 coating, however, it was mechanically stiffer. This is consistent with the vibration-test results, in which the red rubber coating reduced the resonance amplitudes while causing only minor changes in the resonance frequencies. The mechanical characterization therefore confirms that the vibration response of coated thin-walled sheets depends not only on the mass increase caused by the applied coating, but also on the local hardness, stiffness, and creep susceptibility of the coating. However, since the measurements were performed for the same coating systems as those used in the vibration experiments, they provide a direct and physically consistent basis for interpreting the damping behaviour of the investigated coated sheets.

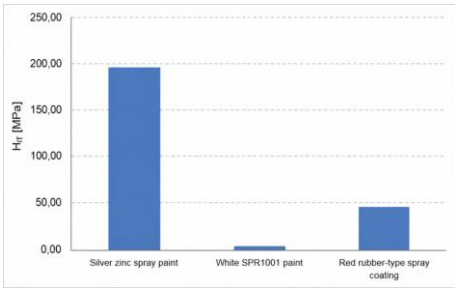


Fig.10. Indentation hardness HIT of the coatings used in the vibration tests: silver zinc spray paint, white SPR1001 paint, and red rubber spray coating.

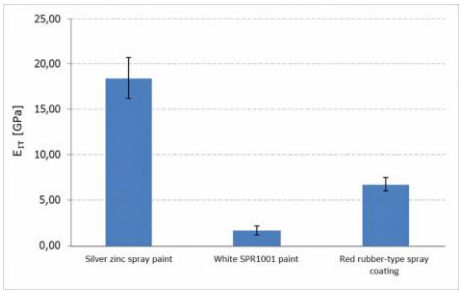


Fig.11. Indentation modulus EIT of the coatings used in the vibration tests: silver zinc spray paint, white SPR1001 paint, and red rubber spray coating.

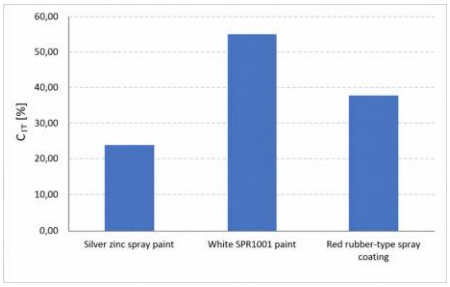


Fig.12. Indentation creep CIT of the coatings used in the vibration tests: silver zinc spray paint, white SPR1001 paint, and red rubber spray coating.

5. NUMERICAL MODAL AND HARMONIC ANALYSIS OF THIN-WALLED STEEL SHEETS WITH DAMPING COATINGS

5.1. Discrete Model and Assumptions

The analyses were performed using the finite element method in the ANSYS environment, assuming a frequency range consistent with the experimental studies, i.e., up to 500 Hz. The geometric model represented a thin-walled steel sheet with dimensions of 40 × 90 × 0.25 mm and uniform thickness, corresponding to the specimens used in the laboratory experiments. The paint coatings were modelled as surface layers applied to one side of the sheet, with each layer assigned a separate set of material properties. The substrate material was defined as isotropic steel with parameters corresponding to electrical steel, including density, Young's modulus, and Poisson's ratio typical for thin-walled steel elements. The properties of the paint coatings were determined based on the experimentally measured mass increase and representative material and damping properties reported in the literature [20],[35],[36] (Table 10). The densities of the layers were selected to reproduce the actual mass increase after the application of one and two paint layers. Material structural damping coefficients were assigned to the coating layers as simplified constitutive parameters. In addition, a global modal damping ratio of 1% was introduced in the harmonic response analysis to represent the overall energy dissipation of the specimen–fixture-exciter system. This approach was adopted as an engineering approximation and was further evaluated through sensitivity analyses. Since

This article has been accepted for publication in a future issue of this journal, but has not been fully edited. Content may change prior to final publication.

experimentally determined frequency-dependent viscoelastic properties of the investigated coatings were not available, the coating layers were represented by homogeneous isotropic materials with constant structural damping coefficients adopted from literature. This simplified representation was intended to reproduce the relative influence of different coating systems on the dynamic response rather than to provide a fully predictive constitutive description. Recent studies also confirm the usefulness of energy-damping assessment and modal analysis for interpreting the dynamic behaviour of layered and beam-like structures [37, 38].

TABLE 10. Material properties used in the numerical model

Material	Density ρ [kg/m³]	Young's modulus E [GPa]	Poisson's Ratio ν	Structural damping coefficient η
Steel	7800	200	0.3	0.002
Zinc paint	2300	2	0.35	0.03
White paint	1593	1	0.35	0.08
Red rubber coating	1200	0.05	0.49	0.15

The global modal damping ratio used in the harmonic response analysis was $\zeta = 0.01$. This parameter was not used in the undamped modal analysis. The global modal damping ratio was used to represent system-level energy dissipation. The structural damping coefficients assigned to the individual materials were retained as approximate constitutive parameters; however, additional calculations showed that reasonable variation of the coating damping coefficients produced negligible changes in the calculated FRFs under the adopted global modal damping assumption. The adopted global modal damping ratio of 1% should be regarded as a representative engineering value rather than an experimentally identified parameter. The boundary conditions were defined to correspond as closely as possible to the experimental configuration. The remaining part of the sheet was left unconstrained, allowing the observation of global bending modes characteristic of thin plates. In the harmonic analysis, the excitation was defined as a harmonic force applied locally at the contact region between the exciter and the free end of the sheet. Shell-type elements were used for discretization, which are suitable for modelling thin-walled structures. A mesh convergence analysis was performed to verify that the calculated natural frequencies were independent of mesh density.

TABLE 11. Mesh convergence analysis of the numerical model.

Mesh size [mm]	f_1 [Hz]	f_2 [Hz]	f_3 [Hz]
5.0	66.50	212.00	413.00
3.0	66.52	212.73	413.09
2.0	66.52	212.73	413.09
1.5	66.52	212.73	413.09

Refining the global element size from 5.0 to 3.0 mm changed the first three natural frequencies by less than 0.4%, while further refinement to 2.0 and 1.5 mm produced no observable changes at the reported precision (Table 11). Consequently, a global element size of 2.0 mm was adopted for all subsequent analyses as a compromise between numerical accuracy and computational cost. The clamped boundary was represented using a fixed support applied over the experimentally clamped region, constraining all translational and rotational degrees of freedom of the shell nodes within this area. The configuration of the numerical model and the adopted boundary conditions are presented in Fig. 13. The final model employed quadratic shell elements with a global element size of 2 mm. The total plate length was 90 mm. Based on the boundary-condition sensitivity analysis, a clamped length of 30 mm was adopted, resulting in a dynamically active free span of 60 mm. A harmonic force with an amplitude of 1 N was applied in the transverse direction over the exciter contact region near the free end. The response was extracted as directional displacement in the excitation direction at the numerical location corresponding to the experimental measurement point. The harmonic analysis was performed from 0.5 to 500 Hz using 1000 solution intervals, corresponding to a frequency resolution of approximately 0.5 Hz. Twenty modes were included in the modal solution used for mode-superposition analysis.

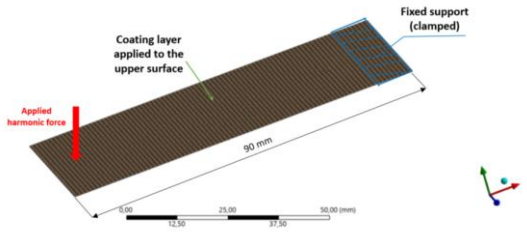


Fig.13. Numerical model of the sheet used in the modal and harmonic analysis together with the applied boundary conditions.

5.2. Modal and harmonic response

In the first stage of the numerical analysis, a modal analysis of the thin-walled steel sheets was performed in order to determine the natural frequencies and the corresponding mode shapes. The calculations were carried out for the base configuration (Clear) and for models including one (Layer 1) and two layers of paint coatings (Layer 2). For the base configuration (Clear), the first natural frequency was 66.52 Hz. Subsequent bending modes occurred at 212.73 Hz, 413.09 Hz, 724.60 Hz, and 924.80 Hz, characterized by an increasing number of vibration nodes. The mode shapes corresponded to classical bending modes of a thin-walled structure and did not exhibit local concentrations of deformation. In the experimental studies, a low-frequency resonance around 25 Hz was recorded. This resonance has a global character and is associated with the compliance of the specimen mounting system and the inertia of the vibration exciter. This phenomenon was not reproduced in the numerical model, where an ideal kinematic clamping condition was assumed,

This article has been accepted for publication in a future issue of this journal, but has not been fully edited. Content may change prior to final publication.

which eliminated the additional degrees of freedom present in the real measurement setup. The mode shapes are presented with scaled displacements in order to improve the clarity of the visualization (Fig. 14).

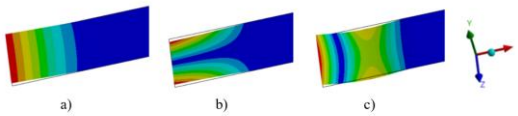


Fig.14. Natural vibration mode shapes of the sheet (Clear state) obtained from the modal analysis: a) Mode I (66.5 Hz), b) Mode II (212.7 Hz), c) Mode III (413.1 Hz)

The first bending mode obtained in the numerical analysis corresponds to the dominant resonance recorded in the FFT amplitude spectra in the experimental measurements. This agreement indicates that the numerical model captures the fundamental bending response of the sheet with satisfactory accuracy for the first experimentally identified resonance. However, the model should be interpreted as a comparative engineering model rather than a fully calibrated representation of the complete experimental setup. The natural frequencies of the first three bending modes for all analysed variants are summarized in Table 12, which enables a direct comparison of the influence of the coating type and the number of layers on the dynamic properties of the sheet. Additionally, the relative change in frequency with respect to the base model (Clear) was determined (in %).

TABLE 12. First three natural frequencies and relative frequency shifts for the analysed coating systems.

Specimen state	Coating	Frequency I [Hz]	Frequency II [Hz]	Frequency III [Hz]	Δf I [%]	Δf II [%]	Δf III [%]
Clear	-	66.52	212.73	413.09	-	-	-
Layer 1	zinc spray paint	66.175	211.62	410.94	-0.52	-0.52	-0.52
Layer 2	zinc spray paint	65.844	210.55	408.88	-1.02	-1.03	-1.02
Layer 1	white SPR1001 paint	64.728	206.95	401.94	-2.69	-2.72	-2.70
Layer 2	white SPR1001 paint	64.353	205.74	399.61	-3.26	-3.29	-3.26
Layer 1	red rubber spray coating	66.318	212.08	411.83	-0.30	-0.31	-0.31
Layer 2	red rubber spray coating	66.117	211.44	410.58	-0.61	-0.61	-0.61

The addition of coating layers produced a systematic decrease in the first three natural frequencies. The largest shifts were obtained for the SPR1001 coating, with reductions of approximately 2.7% for the single-layer configuration and 3.3% for the double-layer configuration. For the zinc coating, the corresponding changes were approximately 0.5% and 1.0%, whereas the rubber coating produced the smallest shifts, approximately 0.3% for Layer 1 and 0.6% for Layer 2. The similar relative changes observed for the first three bending modes indicate a predominantly global mass-loading effect rather than a local stiffness modification. A summary of these results is presented in Table 13.

TABLE 13. Comparison of natural frequencies obtained from the numerical analysis and the experimental measurements

Mode	Numerical frequency [Hz]	Experimental frequency [Hz]	Difference [%]
I	66.52	64–65	2.3
II	212.73	300–308	30.0
III	413.09	389–398	4.8

Good agreement was obtained for the first and third experimentally identified response peaks. The second experimental peak, observed at approximately 300–308 Hz, did not coincide with the second natural frequency predicted for the isolated sheet model. The boundary-condition sensitivity analysis confirmed that the calculated modal frequencies are strongly affected by support representation; however, introducing elastic support shifted the numerical frequencies towards lower values and therefore did not directly reproduce the experimental peak near 300 Hz. This suggests that the experimentally identified response may include a different structural mode or a coupled contribution from the specimen–fixture–exciter system rather than representing exclusively the second bending mode of the isolated sheet. The obtained results indicate that the dominant mechanism by which the coatings influence the dynamic properties of the thin-walled sheet is the mass-loading effect, while the influence on the global stiffness remains secondary. The changes in natural frequencies did not exceed approximately 3.3% for the analysed configurations, which is consistent with literature data concerning thin paint coatings applied to thin-walled metal elements. In the second stage of the numerical investigation, a harmonic response analysis was performed to evaluate the dynamic behaviour of the coated thin-walled steel sheets under sinusoidal excitation. The analysis was carried out using the mode superposition method in the frequency range of 0.5–500 Hz. A unit harmonic force was applied at the free end of the specimen, whereas the response was evaluated as the directional displacement in the excitation direction. To represent the overall energy dissipation of the specimen–fixture–exciter system, a global modal damping ratio of $\zeta = 0.01$ was introduced for all analysed configurations. Under these assumptions, the calculated displacement amplitudes should be interpreted as comparative frequency response functions rather than direct predictions of the experimentally measured vibration amplitudes. The harmonic response functions obtained for the zinc, rubber and SPR1001 coatings are presented in Figs. 15–17. In all analysed cases, the dominant response occurred within the frequency range corresponding to the first bending mode. Increasing the number of coating layers produced a slight shift of the resonance peak towards lower frequencies, in agreement with the trends obtained from the modal analysis. The largest frequency shift was observed for the

This article has been accepted for publication in a future issue of this journal, but has not been fully edited. Content may change prior to final publication.

SPR1001 coating, whereas zinc and rubber coatings produced only minor changes in the resonance position. The response amplitudes remained comparable because the same global modal damping ratio was adopted for all numerical models. The zinc coating produced only a slight reduction in the resonance frequencies. For the single-layer configuration (L1), the first resonance frequency decreased from 66.43 Hz to 65.94 Hz, corresponding to a reduction of approximately 0.75%, whereas the two-layer coating produced a comparable shift. The third resonance frequency decreased from 413.09 Hz to 411.09 Hz (L1) and 409.09 Hz (L2), corresponding to reductions of approximately 0.5% and 1.0%, respectively (Fig. 15). The maximum response amplitudes remained very similar to the reference specimen, ranging from 37.60 mm to 39.39 mm, indicating that the zinc coating primarily influenced the resonance position through a slight increase in structural mass while producing only a negligible effect on the overall dynamic response.

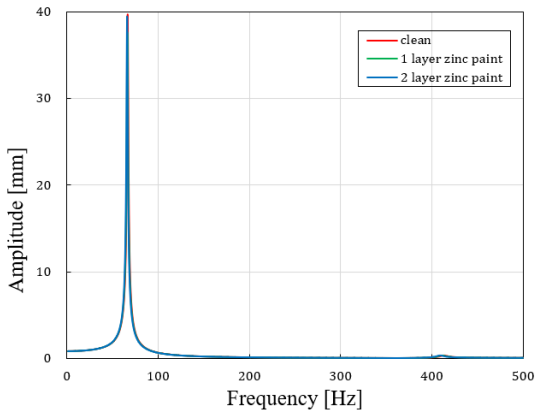


Fig.15. Amplitude–frequency characteristics of the harmonic response for the reference specimen and the specimen with one and two layers of zinc paint

The red rubber coating exhibited behaviour similar to that of the zinc coating (Fig. 16). The first resonance frequency decreased only slightly, from 66.43 Hz to 66.43 Hz (Layer 1) and 65.94 Hz (Layer 2), while the third resonance shifted from 413.09 Hz to 412.09 Hz and 410.59 Hz, respectively. The corresponding reductions did not exceed approximately 0.6%. The maximum response amplitudes remained within a narrow range of 38.59–39.26 mm, demonstrating that the rubber coating caused only minor changes in the predicted harmonic response of the analysed structure.

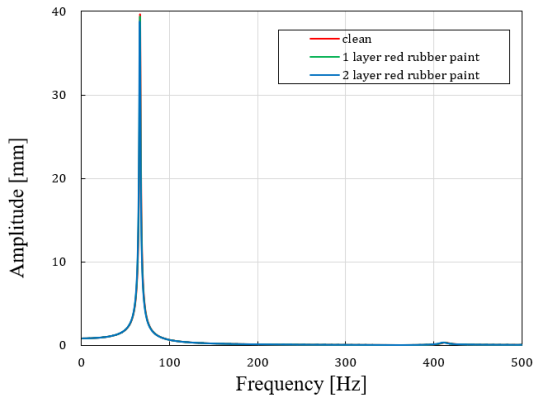


Fig.16. Amplitude–frequency characteristics of the harmonic response for the reference specimen and the specimen with one and two layers of red rubber paint

The largest resonance-frequency shifts were observed for the SPR1001 coating (Fig. 17). The first resonance frequency decreased from 66.43 Hz for the reference specimen to 64.94 Hz for Layer 1 and 64.44 Hz for Layer 2, corresponding to reductions of approximately 2.3% and 3.0%, respectively. Similar trends were observed for the second and third resonance frequencies, with the third resonance decreasing from 413.09 Hz to 402.10 Hz (L1) and 399.60 Hz (L2), corresponding to an overall reduction of approximately 3.3%. Although the resonance frequencies exhibited the largest shift among all analysed coating systems, the peak amplitudes remained relatively close to those obtained for the reference specimen (37.58–39.06 mm). These results indicate that the dominant numerical effect of the SPR1001 coating was the modification of the mass distribution and the associated resonance-frequency shift rather than a substantial change in the predicted response amplitude.

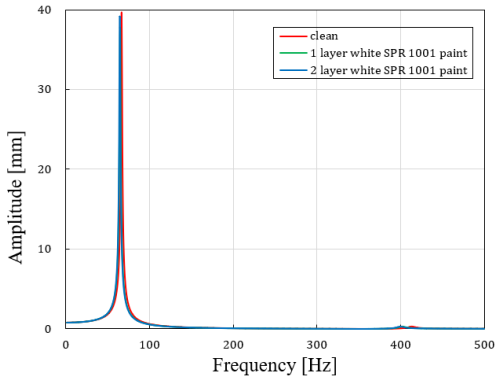


Fig.17. Amplitude–frequency characteristics of the harmonic response for the reference specimen and the specimen with one and two layers of white SPR1001 paint

Fig. 18 and Fig. 19 provide a direct comparison of the harmonic responses obtained for different coating materials applied in one-layer and two-layer configurations. The results clearly demonstrate that the coating material primarily affects the resonance position rather than the overall shape of the

This article has been accepted for publication in a future issue of this journal, but has not been fully edited. Content may change prior to final publication.

frequency response. Among the analysed systems, the SPR1001 coating caused the largest shift of the first and third resonance frequencies, while the zinc and rubber coatings exhibited only minor changes relative to the uncoated specimen. The similarity of the response curves confirms that the global dynamic behaviour of the sheet remained governed by the fundamental bending modes identified in the modal analysis.

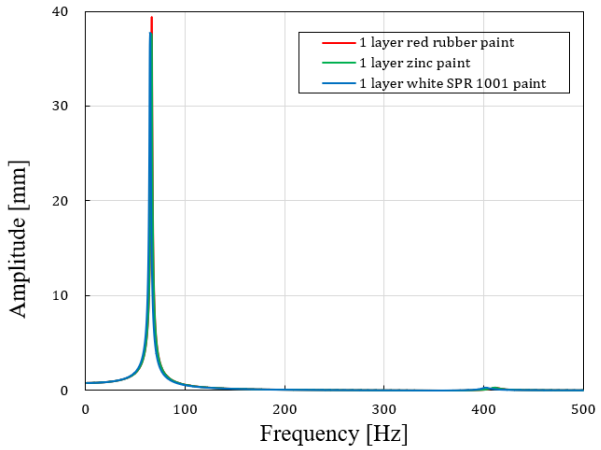


Fig.18. Comparison of the harmonic response for different types of single-layer coatings (Layer 1)

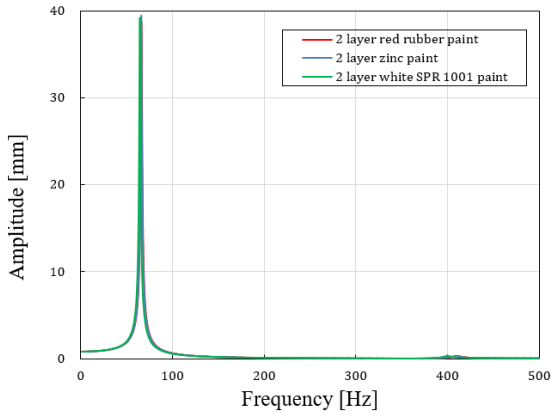


Fig.19. Comparison of the harmonic response for different types of double-layer coatings (Layer 2)

The characteristic resonance parameters extracted from the harmonic response functions are summarized in Table 14. For the uncoated reference specimen (Clear), the dominant resonance occurred at 66.43 Hz, with a maximum directional displacement amplitude of 39.65 mm. The second and third resonance peaks were identified at 180.32 Hz and 413.09 Hz, respectively, with considerably lower response amplitudes of 0.118 mm and 0.308 mm. This confirms that the global dynamic response of the cantilever specimen was governed primarily by the first bending mode.

TABLE 14. Identified harmonic-response peaks and corresponding directional displacement amplitudes.

Variant	f_1 [Hz]	A_1 [mm]	f_2 [Hz]	A_2 [mm]	f_3 [Hz]	A_3 [mm]
Clean	66.434	39.648	180.32	0.11786	413.09	0.30784
Zinc L1	65.935	37.600	180.32	0.11619	411.09	0.30787
Zinc L2	65.935	39.385	180.32	0.11457	409.09	0.30747
Rubber L1	66.434	39.259	180.32	0.11697	412.09	0.30834
Rubber L2	65.935	38.585	180.32	0.11609	410.59	0.30785
SPR1001 L1	64.936	37.575	180.32	0.10914	402.10	0.30566
SPR1001 L2	64.436	39.062	180.32	0.10718	399.60	0.30410

Overall, the harmonic response reproduced the frequency-shift trends identified in the modal analysis, most clearly for the first and third bending modes. The SPR1001 coating produced the largest shifts, reaching approximately 3.0% for the first response peak and 3.3% for the third, whereas the corresponding changes for zinc and rubber remained below approximately 1%. Because a common global modal damping ratio was used, the differences in receptance amplitudes were moderate. The harmonic model is therefore used primarily for comparative assessment of resonance positions and response trends rather than for direct prediction of experimental amplitude levels.

5.3. Sensitivity analysis of the numerical model

A sensitivity analysis was performed to assess the influence of the principal modelling assumptions on the predicted dynamic response. The investigated parameters included the global modal damping ratio, support stiffness, and the Young's modulus of the SPR1001 coating. The mesh convergence study presented in Section 5.1 was also considered as part of the numerical verification procedure.

TABLE 15. Sensitivity analysis of the global modal damping ratio.

Coating	Damping ratio	f_1 [Hz]	A_1 [mm]
Rubber L2	0.005	65.935	70.046
Rubber L2	0.010	65.935	38.585
Rubber L2	0.020	65.935	19.829
SPR1001 L2	0.005	64.436	76.261
SPR1001 L2	0.010	64.436	39.062
SPR1001 L2	0.020	64.436	19.653

The global modal damping ratio was varied between 0.005 and 0.020 for the SPR1001 L2 and rubber L2 configurations (Table 15). The resonance frequencies remained unchanged, indicating that they were governed

This article has been accepted for publication in a future issue of this journal, but has not been fully edited. Content may change prior to final publication.

primarily by the mass and stiffness distributions. In contrast, the first-peak receptance decreased from 70.05 to 19.83 mm for rubber L2 and from 76.26 to 19.65 mm for SPR1001 L2. Thus, increasing the damping ratio by a factor of four reduced the resonance amplitude by approximately the same factor. This result confirms the expected behaviour of a linear damped system and demonstrates that the assumed global damping ratio controls the response magnitude rather than the resonance position. Since the damping ratio primarily affected the response amplitudes while leaving the resonance frequencies unchanged, the next stage focused on the influence of the boundary-condition representation on the modal characteristics (Table 16).

TABLE 16. Sensitivity analysis of the boundary conditions.

Boundary condition	Parameter	f_1 [Hz]	f_2 [Hz]	f_3 [Hz]
Elastic support	0.01 N/mm³	35.203	134.73	202.34
Elastic support	0.1 N/mm³	46.930	169.62	286.40
Elastic support	1.0 N/mm³	54.383	188.15	337.09
Elastic support	10 N/mm³	59.286	198.59	368.34
Fixed support	Ideal	66.520	212.73	413.09

Replacing the ideal fixed support with elastic support produced a systematic decrease in all three natural frequencies. As the support stiffness increased from 0.01 to 10 N/mm³, the first natural frequency increased from 35.20 to 59.29 Hz, while the second and third frequencies increased from 134.73 to 198.59 Hz and from 202.34 to 368.34 Hz, respectively. The results approached, but did not reach, the ideal fixed-support solution. This analysis demonstrates that the boundary-condition representation is one of the dominant sources of uncertainty in the numerical model. However, because compliant support shifted the frequencies downward, it did not directly reproduce the experimentally identified peak near 300–308 Hz. Because the boundary-condition analysis demonstrated a pronounced sensitivity of the natural frequencies to support stiffness, an additional material-parameter study was performed to determine whether uncertainty in the coating stiffness could produce a comparable effect.

TABLE 17. Sensitivity analysis of the Young's modulus of the SPR1001 coating.

E SPR1001 [GPa]	f_1 [Hz]	f_2 [Hz]	f_3 [Hz]
0.5	64.156	205.14	398.39
1.0	64.353	205.74	399.61
1.5	64.548	206.33	400.81

Varying the SPR1001 Young's modulus from 0.5 to 1.5 GPa changed the first three natural frequencies by approximately 0.6% (Table 17). The model is therefore weakly sensitive to moderate uncertainty in coating stiffness, and the observed resonance shifts are governed primarily by coating mass rather than by the assumed Young's modulus. Overall, the sensitivity analysis showed that the boundary-condition representation had the greatest influence on the predicted natural frequencies, whereas the global damping ratio mainly controlled the response amplitude. In contrast, reasonable variations in the SPR1001 Young's modulus produced changes below 1%, indicating that the numerical conclusions are only weakly dependent on the assumed coating stiffness. These results identify support modelling and global damping as the principal sources of uncertainty in the adopted finite element model.

5.4. Limitations and applicability of the numerical model

The numerical model should be interpreted as an engineering comparative model rather than a fully predictive representation of the experimental system. The coatings were represented as homogeneous layers with simplified material damping, and frequency-dependent viscoelastic effects were not included. In addition, the real fixture–specimen–exciter interaction was simplified. However, the mesh convergence, damping sensitivity, boundary-condition sensitivity, and Young's modulus sensitivity analyses demonstrate that the model provides stable and physically consistent trends. Therefore, the model is suitable for comparative assessment of the influence of coating type and layer number on resonance-frequency shifts and overall response trends in thin-walled steel sheets.

Overall, the additional convergence and sensitivity analyses considerably increase the reliability of the numerical model. The mesh convergence study confirmed numerical stability, whereas the damping, boundary-condition, and material-property sensitivity analyses identified the parameters that most strongly influence the predicted response. Consequently, the developed FEM model provides a useful comparative engineering framework for evaluating resonance-frequency shifts and for interpreting the relative influence of coating type and layer number. Quantitative prediction of absolute vibration amplitudes would require experimental identification of damping, frequency-dependent viscoelastic coating properties, and a more detailed representation of the fixture–specimen–exciter interaction.

6. CONCLUSION

The main contribution of this study is the identification of coating-dependent vibration-reduction regimes in thin-walled steel sheets. Although all investigated coatings reduced the resonance amplitudes, they did not act through the same dynamic mechanism. The zinc and red rubber coatings exhibited reductions in vibration amplitudes consistent with increased damping, while causing only minor changes in resonant frequencies. In contrast, the SPR1001 coating produced the strongest amplitude reduction together with the most pronounced decrease in natural frequencies, which indicates a combined damping and mass-loading effect. From a design perspective, this distinction is important because it

This article has been accepted for publication in a future issue of this journal, but has not been fully edited. Content may change prior to final publication.

shows that the choice of coating should depend not only on the expected amplitude reduction, but also on whether resonance retuning is acceptable in the target application. The largest reduction in resonance amplitudes is achieved after the application of the first layer, whereas the second layer usually enhances the effect to a smaller extent. From an application perspective, the selection of the coating should depend on the target frequency band. For maximum reduction of the response around 300 Hz, the SPR1001 coating is the most advantageous. In contrast, when the priority is to reduce amplitude while maintaining minimal changes in resonance frequencies, zinc and red coatings represent suitable solutions. The microhardness results support the interpretation that coating hardness, stiffness, and creep susceptibility contribute to the observed differences in dynamic response. The FEM model reproduced the relative trends in resonance-frequency shifts and therefore provides a useful comparative tool for interpreting the experimental results. The low-frequency experimental component observed near 25 Hz was attributed to the compliance of the specimen–fixture–exciter system and was therefore not reproduced by the idealized finite element model. However, quantitative prediction of vibration amplitudes would require experimentally identified damping properties and a more detailed representation of the specimen–fixture–exciter system. The damping-related interpretation presented in this study is inferred from the experimentally observed reductions in resonance amplitudes and is not based on direct measurements of modal damping ratios or material loss factors.

References

[1] D. J. Ewins, *Modal Testing: Theory, Practice and Application*, 2nd ed. Baldock, UK: Research Studies Press, 2000.

[2] S. S. Rao, *Mechanical Vibrations in SI Units*, 6th ed. Pearson, 2017.

[3] D. Di Maio, P. Castellini, M. Martarelli, S. Rothberg, M. S. Allen, W. D. Zhu, and D. J. Ewins, "Continuous scanning laser vibrometry: A raison d'être and applications to vibration measurements," *Mech. Syst. Signal Process.*, vol. 156, 107573, 2021, doi: 10.1016/j.ymssp.2020.107573.

[4] D. I. G. Jones, *Handbook of Viscoelastic Vibration Damping*. Chichester/New York: Wiley, 2001.

[5] B. J. Lazan, *Damping of Materials and Members in Structural Mechanics*. Oxford/New York: Pergamon Press, 1968.

[6] D. J. Inman, *Engineering Vibration*, 4th ed. Upper Saddle River, NJ: Pearson, 2014.

[7] W. Macek, T. Łagoda, N. Mucha, "Energy-based fatigue failure characteristics of materials under random bending loading in elastic-plastic range," *Fatigue & Fracture of Engineering Materials & Structures*, vol. 41, pp. 249–259, 2018, doi: 10.1111/ffe.12677.

[8] G. Lesiuk, K. Junik, S. Duda, T. Socha, K. Kula, A. Denisiewicz, D. Medyński, W. Macek, J.A.F.O. Correia, "Prediction of the fatigue lifetime of PUR structural elements using a combined experimental-numerical approach," *Structures*, vol. 59, 105822, 2024, doi: 10.1016/j.istruc.2023.105822.

[9] M. I. Żyłka, "The experimental determination of the speed of piston rods of two pneumatic cylinders with a synchronizing element," *Adv. Sci. Technol. Res. J.*, vol. 15, no. 2, pp. 84–89, 2021, doi: 10.12913/22998624/135596.

[10] M. I. Żyłka, Z. Szczerba, and K. Szczerba, "Experimental research on the velocity of two pneumatic drives with an element for concurrent motion," *Adv. Sci. Technol. Res. J.*, vol. 16, no. 2, pp. 81–88, 2022, doi: 10.12913/22998624/145669.

[11] L. Leniowska, "Modelling and vibration control of planar systems by the use of piezoelectric actuators," *Arch. Acoust.*, vol. 34, no. 4, pp. 507–519, 2009.

[12] P. Świrk, J. Żyłka, L. Leniowska, and M. Grochowina, "Vibration reduction assessment of layered acoustic metamaterial," *Vibrations in Physical Systems*, vol. 33, no. 2, 2022, doi: 10.21008/j.0860-6897.2022.2.21.

[13] D. J. Mead, *Passive Vibration Control*. Chichester: Wiley, 1998.

[14] M. D. Rao, "Recent applications of viscoelastic damping for noise control in automobiles and commercial airplanes," *J. Sound Vib.*, vol. 262, no. 3, pp. 457–474, 2003, doi: 10.1016/S0022-460X(03)00106-8.

[15] W. Żyłka, "The investigation of influence of paint coatings on structure vibrations," *Vibrations in Physical Systems*, vol. 35, no. 2, 2024, doi: 10.21008/j.0860-6897.2024.2.06.

[16] E. E. Ungar and E. M. Kerwin, "Loss factors of viscoelastic systems in terms of energy concepts," *J. Acoust. Soc. Am.*, vol. 34, no. 7, pp. 954–957, 1962, doi: 10.1121/1.1918227.

[17] A. D. Nashif, D. I. G. Jones, and J. P. Henderson, *Vibration Damping*. New York: Wiley-Interscience, 1985.

[18] G. C. Everstine and M. S. Marcus, "Finite element prediction of loss factors for structures with frequency-dependent damping treatments," in *Thirteenth NASTRAN Users' Colloquium (NASA-CP-2373)*, NASA NTRS, Document ID: 19850017578, 1985.

[19] M. I. Żyłka, W. Żyłka, Z. Szczerba, and M. Biskup, "An original system for controlling the speed of movement of pneumatic drives in rehabilitation devices," *Adv. Sci. Technol. Res. J.*, vol. 17, no. 1, pp. 124–132, 2023, doi: 10.12913/22998624/157250.

[20] F. Wang, J. Liao, C. Huang, H. Yu, J. Yan, and H. Li, "Study on the damping dynamics characteristics of a viscoelastic damping material," *Processes*, vol. 10, no. 4, 635, 2022, doi: 10.3390/pr10040635.

[21] J. Huang et al., "Influence of crosslinking density on the mechanical and thermal properties of plant oil-based epoxy resin," *RSC Adv.*, vol. 12, pp. 23048–23056, 2022, doi: 10.1039/D2RA04206A.

[22] M. Żyłka, W. Żyłka, K. Klukowski, "Technical solutions enabling the physical training of astronauts during long-term stays at space stations," *Adv. Sci. Technol. Res. J.*, vol. 17, no. 4, pp. 36–45, 2023, doi: 10.12913/22998624/167935.

[23] L. Yu, Y. Ma, C. Zhou, and H. Xu, "Damping efficiency of the coating structure," *Int. J. Solids Struct.*, vol. 42, no. 11–12, pp. 3045–3058, 2005, doi: 10.1016/j.ijsolstr.2004.10.033.

[24] J. B. Kosmatka and S. L. Liguore, "Review of methods for analyzing constrained-layer damped structures," *J. Aerosp. Eng.*, vol. 6, no. 3, pp. 268–283, 1993, doi: 10.1061/(ASCE)0893-1321(1993)6:3(268).

[25] A. Jackstadt, W. V. Liebig, and L. Kärger, "Analytical modeling and investigation of constrained layer damping in hybrid laminates based on a unified plate formulation," *Int. J. Mech. Sci.*, vol. 216, 106964, 2022, doi: 10.1016/j.ijmecsci.2021.106964.

[26] G. Jin et al., "Preparation of a superior damping coating and study on vibration damping properties," *SN Appl. Sci.*, vol. 5, 218, 2023, doi: 10.1007/s42452-023-05451-3.

[27] J. Wang, T. Guo, W. Liu, Z. Wang, and Y. Zhang, "Vibration analysis and damping effect of blade-hard coating composite structure based on base excitation," *Materials*, vol. 16, 5432, 2023, doi: 10.3390/ma16155432.

[28] G. C. Everstine and M. S. Marcus, "Finite element prediction of loss factors for structures with frequency-dependent damping treatments," in *Thirteenth NASTRAN Users' Colloquium (NASA-CP-2373)*, NASA NTRS, Document ID: 19850017578, 1985.

[29] G. Jin et al., "Preparation of a superior damping coating and study on vibration damping properties," *SN Appl. Sci.*, vol. 5, 220, 2023, doi: 10.1007/s42452-023-05451-3.

[30] A. Szeleziński, A. Muc, L. Murawski, M. Kluczyk, and T. Muchowski, "Application of laser vibrometry to assess defects in ship hull's welded joints' technical condition," *Sensors*, vol. 21, no. 3, 895, 2021, doi: 10.3390/s21030895.

[31] K. Szemela, W. Rdzanek, and W. Żyłka, "The radiation efficiency measurements of real system of a thin circular plate embedded into a thick square baffle," *Arch. Acoust.*, vol. 43, no. 3, pp. 413–423, 2018, doi: 10.24425/123913.

[32] I. Robertson and M. Padaon, "Liquid applied sound damping for high frequency vibrations," *SAE Int. J. Adv. Current Pract. Mobility*, vol. 4, no. 2, pp. 431–437, 2022, doi: 10.4271/2021-01-1123.

[33] M. Żyłka, B. Cieniek, P. Skała, W. Żyłka, and I. Stefaniuk, "Assessment of polyurethane seal degradation in pneumatic drives using EPR and SEM techniques," *Measurement*, vol. 257, 118614, 2026, doi: 10.1016/j.measurement.2025.118614.

This article has been accepted for publication in a future issue of this journal, but has not been fully edited. Content may change prior to final publication.

[34] ISO 14577-1:2015, *Metallic materials—Instrumented indentation test for hardness and materials parameters—Part 1: Test method*. Geneva, Switzerland: ISO, 2015.
[35] Spinks, G.M., Liu, Z., Brown, H.R., Swain, M.V. (2004). Paint layer thermomechanical properties determined by in situ dynamic mechanical analysis in 3-point bending. Progress in Organic Coatings, 49(2), 95–102. DOI: 10.1016/j.porgcoat.2003.09.001.
[36] Zhou, X.Q., Yu, D.Y., Shao, X.Y., Zhang, S.Q., Wang, S. (2016). Research and applications of viscoelastic vibration damping materials: A review. Composite Structures, 136, 460–480. DOI: 10.1016/j.compstruct.2015.10.014.
[37] I. Yavuz, B. Senol, and E. Simsir, "Examination of energy damping behaviour of fiberglass reinforced sandwich structures with extruded polystyrene core material," *Bull. Pol. Acad. Sci.: Tech. Sci.*, vol. 73, no. 3, e153430, 2025, doi: 10.24425/bpasts.2025.153430.
[38] E. Z. Sensoy and T. Baran, "Modal analyses of nonuniform axially functionally graded Euler–Bernoulli beams," *Bull. Pol. Acad. Sci.: Tech. Sci.*, vol. 74, no. 2, e157320, 2026, doi: 10.24425/bpasts.2026.157320.

This article has been accepted for publication in a future issue of this journal, but has not been fully edited. Content may change prior to final publication.